21. Yüzyılda Fen ve Teknik Dergisi
ISSN: 2587-0327 2025, Cilt/Volume: 12, Sayı/Issue: 23, 18-38
Research Article / Araştırma Makalesi Received: 18.11.2023; Accepted: 19.04.2025

Analysis of Linear and Non-Linear Effective Factors on The Projectile Trajectory

Mohammad Zia Zahedi[1]*, Mohammad Ali Sultani[1]

Abstract: Catching projectiles using robotic systems poses significant challenges in robotics research. Understanding the projectile's trajectory and identifying the key factors influencing its movement are fundamental tasks in this field. This study aims to comprehensively analyze the factors affecting the motion of a projectile, specifically focusing on the trajectory of a ping pong ball. Both linear factors, such as gravity, buoyancy force, and centrifugal force, and nonlinear factors like air drag and Coriolis force, are examined. The motion equations of the ping pong ball are solved using numerical and analytical methods implemented in MATLAB programming. The study quantifies the percentage impact of these significant factors on the ball's motion and trajectory. By understanding the contributions of each factor, a more accurate and comprehensive understanding of the projectile's behavior can be achieved. To determine the point of impact of the projectile with the target, an equation of a fitted parabolic curve above the trajectory curve is obtained. This equation provides valuable insights into predicting the precise point of impact with the target. The proposed method is confirmed through the comparison and detailed analysis of the results obtained from analytical and numerical calculations. The findings of this research have broad applications in various fields, including image-based surveillance systems, analysis of sports video images, monitoring human activities, and enhancing human-machine interaction. By considering and studying all significant factors affecting projectile motion, this research contributes to the advancement of robotics research, providing valuable insights and tools for catching projectiles accurately and efficiently. As a result of the study, the effect of gravitational force of the Earth, drag force for laminar flow, drag force for turbulent flow, buoyancy force, centrifugal force, and Coriolis force are 100%, 0.18%, 55.88%, 1.49%, 0.28% and 0.0086% respectively.

Keywords: Nonlinear equations, Dynamics of projectile motion, Air drag, Buoyancy force, Numerical method..

[1]Address: Kabul Polytechnic University, Faculty of Electro-mechanic, Kabul/Afghanistan.

***Corresponding author**: mzzahedi@gmail.com

Citation: Zahedi, M. Z., Sultani, M. A. (2025). Analysis of Linear and Non-linear Effective Factors on The Projectile Trajectory. 21. Yüzyılda Fen ve Teknik Dergisi, 12(23): 18-38.

1. INTRODUCTION

One of the most persistent challenges in robotics research is enabling autonomous systems to reliably grasp dynamic objects in unstructured environments (Kim et al., 2014; Bohg et al., 2014). Achieving this requires the seamless integration of advanced

functionalities, including real-time environmental perception (Bohg et al., 2014), high-speed object tracking, motion estimation, and adaptive path planning (Koval et al., 2015). A key aspect to these tasks is the accurate estimation of projectile trajectories, particularly under real-world constraints such as limited sensor data and computational latency (Cigliano et al., 2015; Kao et al., 2017; Lai & Ke, 2019; Oka et al., 2017). While multi-camera systems have traditionally been employed for 3D trajectory reconstruction (Kao & Ho, 2021; Xie et al., 2014), recent advances in monocular vision algorithms now enable robust estimation using a single camera (Cigliano et al., 2015; Nobahar, 2020; Redmon et al., 2016; Zhang et al., 2020), reducing hardware complexity and computational overhead. However, achieving precision in such setups necessitates rigorous modeling of the physical factors governing projectile motion, a task complicated by the trade-offs between model fidelity and real-time applicability (Kao & Ho, 2021).

Projectile dynamics are traditionally simplified by neglecting secondary forces such as aerodynamic spin-induced Magnus effects (Elger et al., 2020; Nathan, 2008) and non-inertial Coriolis forces (Greenwood, 2003), with many studies focusing solely on gravity and quadratic air resistance (Frese et al., 2001; Lippiello et al., 2013; Nagurka, 2003; Nobahar, 2020; Tian et al., 2011). However, this simplification introduces errors in scenarios involving lightweight objects (e.g., ping-pong balls) or extended trajectories, where buoyancy (Kao & Ho, 2021; Nagurka, 2003; Tian et al., 2011), Reynolds-number-dependent drag (Anderson, 2017; Frese et al., 2001), and centrifugal forces (Goldstein et al., 2001) become non-negligible. So that omitting buoyancy and nonlinear drag in ping-pong ball trajectory models leads to deviations in real-world robotic interception tasks. Brancazio (1985) emphasized the critical role of aerodynamic interactions in sports projectiles, underscoring the need for physics-informed models in robotics.

When a projectile is launched, it is governed by gravitational acceleration, which dominates vertical displacement (Halliday et al., 2013), and buoyancy, which reduces effective weight via Archimedes' principle. Aerodynamic drag—modeled as Stokes' law at low Reynolds numbers or quadratic drag at higher velocities (Batchelor, 2000)—dissipates kinetic energy, while the Magnus effect introduces lateral deflection for spinning objects. Earth's rotational effects, such as the Coriolis force, further perturb long-range trajectories (Greenwood, 2003), though these are often negligible in short-range robotic applications. Despite gravity's dominance, oversimplified models risk introducing substantial inaccuracies, underscoring the necessity of high-fidelity models in robotic systems(Kao & Ho, 2021).

In this study, we develop a comprehensive framework for estimating the trajectory of ping-pong balls in robotic interception tasks, combining both linear (gravity, buoyancy) and nonlinear (quadratic drag, Coriolis force) dynamics. While analytical solutions for such coupled systems are often intractable (Parker, 1997), numerical methods like adaptive Runge-Kutta integration (Press et al., 2007) enable efficient approximations. Prior robotics studies frequently assume parabolic trajectories (Bäuml et al., 2010; Frese et al., 2001; Park, 2009) and model the trajectory of a flying ball as a parabola and refine it iteratively using recursive least squares optimization (Hong & Slotine, 2005; Riley & Atkeson, 2002)—an assumption valid only in idealized, drag-free scenarios (Halliday et al., 2013). Here, we propose a modified parabolic model augmented with empirical drag coefficients, aligning with hybrid analytical-numerical approaches advocated in recent literature (Kao & Ho, 2021; Koval et al., 2015). Our work bridges gaps between idealized

physics models and real-world robotic constraints, offering insights applicable to dynamic grasping, aerial robotics, and sports automation.

2. MATERIAL AND METHOD

2.1. Analytical Method

First, we will examine the analytical method for solving the problem. According to Figure 1, we consider the Cartesian state variables system on the surface of the Earth's northern hemisphere in Kabul. The unit vector $\hat{\mathbf{i}}$ represents the x-direction towards the south, $\hat{\mathbf{j}}$ represents the y-direction towards the east, and $\hat{\mathbf{k}}$ represents the z-direction perpendicular to the surface of the Earth and pointing upwards.

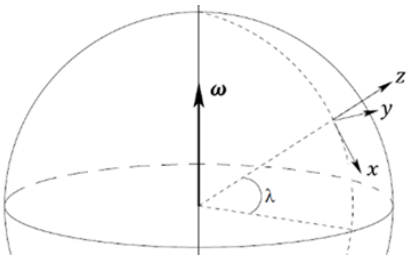

Figure 1. Representation of Cartesian coordinate system.

A represents the geographical latitude of Kabul. In this context, a projectile body, such as a ping pong ball, is considered. Since the motion of the projectile is analyzed with respect to a reference frame that has rotational motion, this system is a non-inertial system for calculation purposes.

The effect of each of these forces on the motion of the ping pong ball projectile is examined:

Gravity force

Considering the effect of gravity as the dominant force, we can describe the governing dynamic equation for the projectile's motion, neglecting the effects of air resistance, buoyancy force, and non-inertial forces. This equation relates the mass (m) and acceleration ($\boldsymbol{a}$) of the projectile under the influence of the Earth's gravitational force, $\boldsymbol{F}_{\mathbf{g}}$. If the projectile starts its motion from position $\boldsymbol{r}_0 = [x_0\ y_0\ z_0]^{\mathrm{T}}$ with an initial velocity $\boldsymbol{v}_0 = \left[v_{x0}\ v_{y0}\ v_{z0}\right]^{\mathrm{T}}$, the equation can be expressed as:

$$\begin{aligned} m\boldsymbol{a} &= \boldsymbol{F}_{\mathbf{g}} = m\mathbf{g}_0 \\ \boldsymbol{a} &= \mathbf{g}_0 = -\mathrm{g}_0\hat{\mathbf{k}} \end{aligned} \tag{1}$$

In equation (1), g_0 is the acceleration of gravity as measured by a nonrotating observer at the surface of Kabul. Therefore, the vertical component of motion experiences a constant acceleration, while the horizontal components have constant velocities. This is because the gravitational force acts vertically downward and does not affect the horizontal motion of the projectile, assuming no other forces are present.

In the motion with constant acceleration, the components of the acceleration vector $\boldsymbol{a} = d\boldsymbol{v}/dt$, velocity vector $\boldsymbol{v}$, and position vector $\boldsymbol{r}$ at time t in the Cartesian coordinate system are given by $\boldsymbol{a} = [0\ 0\ a_z]^{\mathrm{T}}$, $\boldsymbol{v} = \left[v_x\ v_y\ v_z\right]^{\mathrm{T}}$ and $\boldsymbol{r} = [x\ y\ z]^{\mathrm{T}}$ respectively.

These components can be obtained according to the following equations (2):

$$\begin{aligned} & a_z = -\mathrm{g}_0 \\ & \begin{cases} v_x = v_{x0} \\ v_y = v_{y0} \\ v_z = v_{z0} + a_z t \end{cases} \\ & \begin{cases} x = x_0 + v_{x0} t \\ y = y_0 + v_{y0} t \\ z = z_0 + v_{z0} t + (1/2) a_z t^2 \end{cases} \end{aligned} \tag{2}$$

The effect of air resistance

If it is not possible to neglect air resistance acting on the projectile, the Reynolds number $\mathrm{Re} = \rho v L/\mu$ should be examined. In this analysis, μ represents the dynamic viscosity of air, ρ is the density of air, and L is the characteristic length of the projectile. For a spherical body, L is typically taken as the diameter (Çengel & Ghajar, 2011).

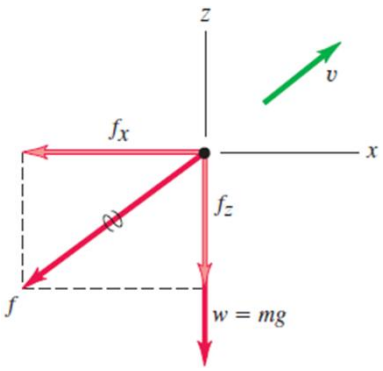

Figure 2. Illustrates that the air resistance force always acts in the opposite direction to the motion of the projectile (Dickhoff, 2023).

If the Reynolds number is less than one, the air resistance behaves as a laminar layer, and according to Stokes' law, the drag force can be expressed as $\boldsymbol{F}_{\mathrm{drag}} = -b\boldsymbol{v} = -(6\pi\mu R)\boldsymbol{v}$ where R is the radius of the spherical body (Parker, July 1997). In this case, the dynamic equation of motion and acceleration of the projectile can be determined accordingly.

$$\begin{aligned} m\boldsymbol{a}_{\mathrm{drag}} &= m\mathbf{g}_0 - b\boldsymbol{v} \\ \boldsymbol{a}_{\mathrm{drag}} &= -\left((b/m)\boldsymbol{v} + \mathrm{g}_0\hat{\mathbf{k}}\right) \\ &= -(b/m)\left(\boldsymbol{v} + v_t\hat{\mathbf{k}}\right) \end{aligned} \tag{3}$$

The components of the acceleration vector of the projectile can be obtained according to the following equations:

$$\begin{cases} a_x = -(b/m)v_x \\ a_y = -(b/m)v_y \\ a_z = -(b/m)(v_z + v_t) \end{cases} \tag{4}$$

The velocity of the projectile, when the effect of gravity is neutralized by air resistance and reaches a constant value, is called the terminal velocity. It can be calculated using the equation $v_t = mg_0/b$, where v_t is the terminal velocity, m is the mass of the projectile, and b is the drag coefficient.

The analytical solution for the differential equation (3) of velocity with respect to time is obtained as follows:

$$\begin{aligned} \frac{d\boldsymbol{v}}{\boldsymbol{v} + v_t\hat{\mathbf{k}}} &= -(b/m)dt \\ \boldsymbol{v} + v_t\hat{\mathbf{k}} &= \left(\boldsymbol{v_0} + v_t\hat{\mathbf{k}}\right)e^{-(b/m)t} \\ \boldsymbol{v} &= -v_t\hat{\mathbf{k}} + \left(\boldsymbol{v_0} + v_t\hat{\mathbf{k}}\right)e^{-(b/m)t} \end{aligned} \tag{5}$$

The velocity equation, in the case where $(b/m)t \ll 1$, can be transformed using the approximation $e^{-(b/m)t} \approx 1 - (b/m)t$ as follows:

$$\boldsymbol{v} = \boldsymbol{v_0} - (b/m)\left(\boldsymbol{v_0} + v_t\hat{\mathbf{k}}\right)t \tag{6}$$

The velocity of an object in free fall with an initial velocity $\boldsymbol{v_0} = 0$ can be obtained from equation (5) as follows:

$$\boldsymbol{v} = -\left(1 - e^{-(b/m)t}\right)v_t\hat{\mathbf{k}} \tag{7}$$

If the Reynolds number is greater than one and less than 10^5, the air resistance on a body is turbulent flow and can be calculated using the quadratic velocity relationship given by the equation $\boldsymbol{F}_{\text{drag}} = -Dv\boldsymbol{v} = -(C_D\rho A/2)v\boldsymbol{v}$ (Parker, 1997). Here, C_D represents the drag coefficient, and $A = \pi R^2$ is the cross-sectional area of the sphere (where R is the radius of the spherical body). Therefore, the nonlinear dependent equations of projectile motion dynamics and its acceleration are obtained as follows:

$$\begin{aligned} m\boldsymbol{a}_{\text{drag}} &= m\mathbf{g}_0 - Dv\boldsymbol{v} \\ \boldsymbol{a}_{\text{drag}} &= -\left((D/m)v\boldsymbol{v} + g_0\hat{\mathbf{k}}\right) = -(D/m)\left(v\boldsymbol{v} + v_t^2\hat{\mathbf{k}}\right) \end{aligned} \tag{8}$$

In this case, the terminal velocity can be obtained using the equation $v_t = \sqrt{mg_0/D}$. The components of the acceleration vector of the projectile at time t can be obtained as follows:

$$\begin{cases} a_x = -(D/m)vv_x \\ a_y = -(D/m)vv_y \\ a_z = -(D/m)(vv_z + v_t^2) \end{cases} \tag{9}$$

Due to the challenging nature of finding a general analytical solution for these nonlinear dependent equations, this paper presents a numerical solution for them. However, in this specific article, analytical solutions have been investigated for certain special cases. In the case of free fall, the analytical solution for the vertical component of equations (9) is given by:

$$v_z = -v_t tanh\left(\frac{g_0 t}{v_t}\right) \tag{10}$$

Alternatively, in the case of vertical projectile motion with an initial velocity $v_{z0}\hat{\mathbf{k}}$, the analytical solution for the vertical component of equations (9) is given as (Naguraka, 2003).

$$v_z = v_t tan\left[tan^{-1}\left(\frac{v_{z0}}{v_t}\right) - \frac{g_0 t}{v_t}\right] \tag{11}$$

Alternatively, in the case of horizontal motion with an initial velocity $\boldsymbol{v}_0 = v_{x0}\hat{\mathbf{i}}$, only the x-component of equation (9) is considered, and its analytical solution is straightforwardly obtained.

$$\begin{aligned} a_x &= -(D/m)v_x^2 \\ \frac{dv_x}{v_x^2} &= -(D/m)dt \\ v_x &= \frac{v_{x0}}{1 + t/\tau} \end{aligned} \tag{12}$$

where $\tau = m/(Dv_{x0})$.

From the recent equation, one can obtain the position of the object with respect to the origin, considering the start of motion, as follows

$$x = v_{x0}\tau \ln(1 + t/\tau) \tag{13}$$

The effect of buoyancy force

Considering the buoyancy force of the air as $\boldsymbol{F}_\mathrm{b} = \rho V g_0 \hat{\mathbf{k}}$, where ρ is the density of air, $V = \frac{4}{3}\pi R^3$ is the a spherical body volume and R is the radius, the dynamic equations for the motion and acceleration of the projectile can be obtained as follows

$$\begin{aligned} m\boldsymbol{a}_\mathrm{b} &= m\mathbf{g}_0 + \rho V g_0 \hat{\mathbf{k}} = -m' g_0 \hat{\mathbf{k}} \\ \boldsymbol{a}_\mathrm{b} &= -(m'/m) g_0 \hat{\mathbf{k}} \end{aligned} \tag{14}$$

Since the acceleration of the projectile is constant, the components of the acceleration vector, velocity, and position of the projectile at time t are obtained in a similar manner as equations (2).

$$\begin{aligned} a_z &= -(m'/m) g_0 \\ &\begin{cases} v_x = v_{x0} \\ v_y = v_{y0} \\ v_z = v_{z0} + a_z t \end{cases} \\ &\begin{cases} x = x_0 + v_{x0} t \\ y = y_0 + v_{y0} t \\ z = z_0 + v_{z0} t + (1/2) a_z t^2 \end{cases} \end{aligned} \tag{15}$$

where $m' = m - \rho V$.

The effect of centripetal force

In addition to the gravitational force, a body moving relative to the Earth experiences non-inertial forces due to the Earth's rotational motion, including the centrifugal force and the Coriolis force. The direction of the angular velocity $\boldsymbol{\omega}$ of the Earth's rotational motion is from south to north along the axis of rotation. From the perspective of an observer rotating with the Earth, the acceleration of the body can be obtained from the following equation

$$\mathbf{g} = \mathbf{g}_0 - 2\boldsymbol{\omega} \times \boldsymbol{V}' - \boldsymbol{\omega} \times (\boldsymbol{\omega} \times \boldsymbol{r}) \tag{16}$$

where $r = R_\mathrm{E}$ is the radius of the Earth. If we neglect the effects of the Coriolis acceleration $-2\boldsymbol{\omega} \times \boldsymbol{V}'$ compared to the centripetal acceleration $-\boldsymbol{\omega} \times (\boldsymbol{\omega} \times \boldsymbol{r})$, the effective gravitational acceleration $\mathbf{g}$ can be expressed as:

$$\mathbf{g} = \mathbf{g}_0 - \boldsymbol{\omega} \times (\boldsymbol{\omega} \times \boldsymbol{r}) \tag{17}$$

The direction of this acceleration and its components are shown in Figure 3 and Figure 4.

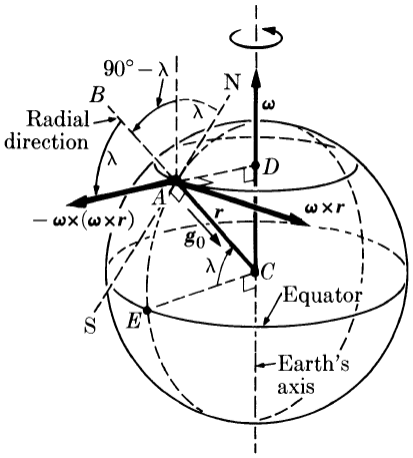

Figure 3. Illustrates the centrifugal acceleration in the northern hemisphere due to the Earth's rotational motion (Alonso & Finn, 1967).

Taking into account the radius and angular velocity of the Earth, the value of the centrifugal acceleration with respect to the geographical latitude can be obtained as follows (Alonso & Finn, 1967).

$$\begin{aligned} |-\boldsymbol{\omega} \times (\boldsymbol{\omega} \times \boldsymbol{r})| &= r\omega^2 \cos(\lambda) \\ &= 3.34 \times 10^{-2} \cos(\lambda) \end{aligned} \tag{18}$$

The maximum value of this acceleration occurs at the equator and is about %0.3 acceleration of the Earth's gravity, g_0.

According to Figure 4, the components of the radial and tangential accelerations due to the centrifugal force can be calculated as follows

$$-\boldsymbol{\omega} \times (\boldsymbol{\omega} \times \boldsymbol{r}) = r\omega^2 \cos(\lambda)\left(\sin(\lambda)\hat{\mathbf{i}} + \cos(\lambda)\hat{\mathbf{k}}\right) \tag{19}$$

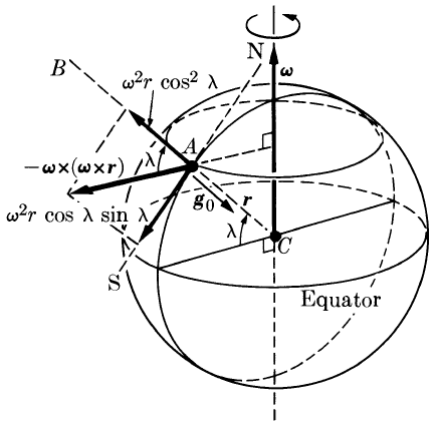

Figure 4. Shows the components of the radial and tangential accelerations due to the Earth's rotational motion in the northern hemisphere (Alonso & Finn, 1967).

And the vector of the effective gravitational acceleration, **g**, can be obtained as follows

$$\begin{aligned} \mathbf{g} = r\omega^2 \cos(\lambda)\sin(\lambda)\hat{\mathbf{i}} \\ + \left(-g_0 + r\omega^2 \cos^2(\lambda)\right)\hat{\mathbf{k}} \end{aligned} \tag{20}$$

Therefore, the effective acceleration is given as follows

$$\mathbf{g} = [0\ 0.016\ 0\ -9.772]^{\mathrm{T}} \tag{21}$$

Therefore, the value of $\mathbf{g}$ is $g = 9.772\ \mathrm{m/s^2}$, and its deviation angle from the radial direction of the Earth is $0.0925°$. The north-south component of the effective acceleration is small, but it provides the launching deviation towards the south. Figure 5 illustrates the definition of vertical plumb line and the components of the effective acceleration in the northern hemisphere of the Earth. Figure 6 shows the deviation towards the south in the free fall of an object in the northern hemisphere of the Earth due to the eastward component of the effective acceleration (**î**).

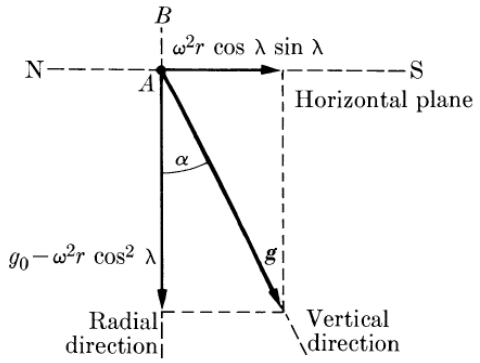

Figure 5. Depicts the definition of the vertical plumb line and the effective acceleration in free fall in the northern hemisphere of the Earth (Alonso & Finn, 1967).

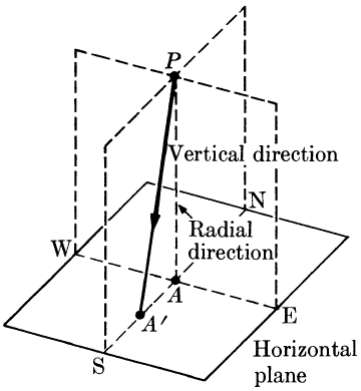

Figure 6. Illustrates the deviation of the plumb line towards the south in the free fall of an object in the northern hemisphere of the Earth due to the centrifugal acceleration (Alonso & Finn, 1967).

Therefore, the components of the acceleration vector, velocity, and position of the projectile at time t can be obtained in a similar manner as equations (2):

$$\begin{cases} a_x = r\omega^2\cos(\lambda)\sin(\lambda) \\ a_y = 0 \\ a_z = r\omega^2\cos^2(\lambda) \end{cases} \qquad \begin{cases} v_x = v_{x0} + a_x t \\ v_y = v_{y0} \\ v_z = v_{z0} + a_z t \end{cases} \tag{22}$$

$$\begin{cases} x = x_0 + v_{x0}t + (1/2)a_x t^2 \\ y = y_0 + v_{y0}t \\ z = z_0 + v_{z0}t + (1/2)a_z t^2 \end{cases}$$

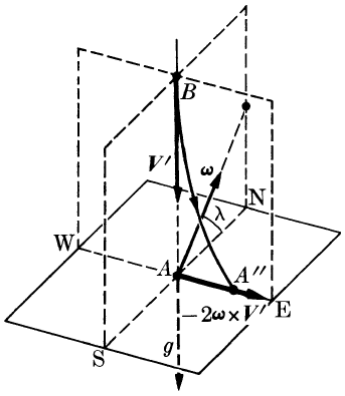

Figure 7. Illustrates the eastward deflection of a freely falling object in the northern hemisphere of the Earth due to the Coriolis acceleration (Alonso & Finn, 1967).

The effect of the Coriolis force

If we consider only the effect of the Coriolis force, the projectile's acceleration can be expressed as follows:

$$\boldsymbol{a} = \mathbf{g}_0 - 2\boldsymbol{\omega} \times \boldsymbol{V'} \tag{23}$$

In the case of free fall, the velocity $\boldsymbol{V'}$ is directed downward, and according to Figure 7, the direction of the Coriolis acceleration $-2\boldsymbol{\omega} \times \boldsymbol{V'}$ is towards the east. Therefore, in free fall, the object is deflected towards the east.

When an object moves on a horizontal plane, the Coriolis acceleration has two components: horizontal and vertical. The horizontal component of the Coriolis acceleration causes the object to move towards the right direction in the northern hemisphere of the Earth (Figure 8).

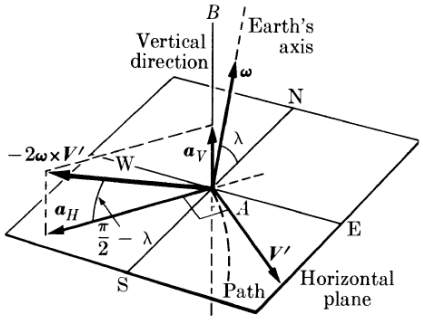

Figure 8. Shows that when an object moves on a horizontal plane in the northern hemisphere of the Earth, the horizontal component of the Coriolis acceleration causes the object to move towards the right direction (Alonso & Finn, 1967).

Therefore, the components of the projectile's acceleration vector at time t can be obtained as follows:

$$\begin{cases} a_x = -(2\boldsymbol{\omega} \times \boldsymbol{V'})_x \\ a_y = -(2\boldsymbol{\omega} \times \boldsymbol{V'})_y \\ a_z = \mathbf{g}_0 - (2\boldsymbol{\omega} \times \boldsymbol{V'})_z \end{cases} \tag{24}$$

2.2. Numerical Method

The motion of a projectile is influenced by the gravitational force of the Earth, buoyancy force, and centrifugal force, which result in a constant acceleration. However, the projectile's acceleration is variable due to the influence of air resistance or the Coriolis force. By choosing a sufficiently small time interval Δt, the projectile's acceleration under the influence of these factors can be considered constant. The values of acceleration under different influences are provided in Table 2.

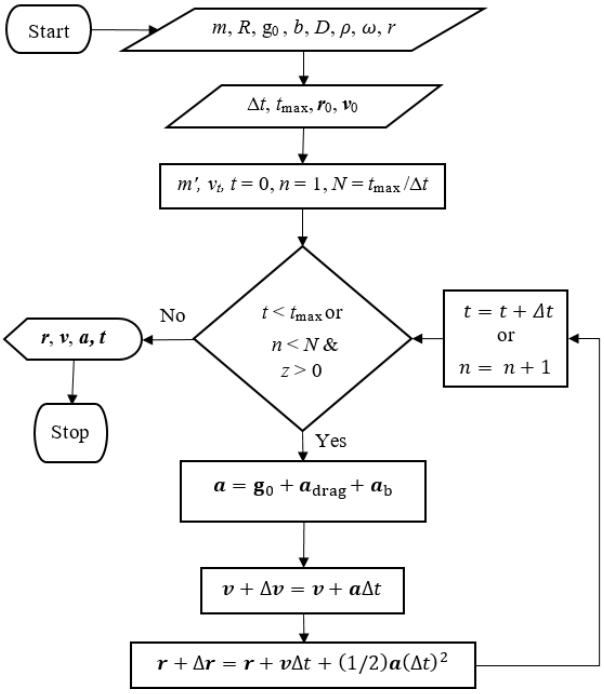

Figure 9. Represents the flowchart of the algorithm for numerically solving the kinematic equations of projectile motion.

Therefore, given the position and velocity of the projectile at time t, they can be obtained at time $t + \Delta t$ using the equations of motion with constant acceleration. Within the time interval Δt, the average acceleration is $\boldsymbol{a} = \Delta \boldsymbol{v}/\Delta t$, and the change in velocity is $\Delta \boldsymbol{v} = \boldsymbol{a}\Delta t$. Hence, the velocity at the end of the time interval Δt becomes:

$$\boldsymbol{v} + \Delta \boldsymbol{v} = \boldsymbol{v} + \boldsymbol{a}\Delta t \tag{25}$$

And the position of the projectile at the end of the time interval Δt is obtained from this equation

$$\boldsymbol{r} + \Delta \boldsymbol{r} = \boldsymbol{r} + \boldsymbol{v}\Delta t + (1/2)\boldsymbol{a}(\Delta t)^2 \tag{26}$$

Therefore, the flowchart of the algorithm for solving the kinematic equations of projectile motion follows the sequence shown in Figure 9.

It goes without saying that the change in the position of the object occurs in the form of a parabola only within the time interval Δt. However, due to the influencing factors on its motion, it is possible that the trajectory of the projectile within a large time interval may not be a perfect parabola.

Table 1. Necessary quantities and their values used in the calculations(Nagurka, 2003).

Quantity	**Symbol**	**Value**
The acceleration of gravity as measured by a nonrotating observer at the surface of Kabul	g_0	$9.8\ \mathrm{m/s^2}$
The elevation of the cable relative to sea level	h	1791 m
The acceleration due to gravity at the surface of Kabul, neglecting the effect of centrifugal force	g	$9.795\ \mathrm{m/s^2}$
The acceleration due to gravity at the surface of Kabul, considering the effect of centrifugal force	g	$9.772\ \mathrm{m/s^2}$
The geographic latitude of Kabul	λ	34.5553^{o}
The mass of the ping pong ball (Naguraka, 2003)	m	2.7 g
The diameter of the ping pong ball (Naguraka, 2003)	L	40.0 mm
The dynamic viscosity of air at 20ºC (Çengel & Ghajar, 2011)	μ	1.8×10^{-5} $\mathrm{kg/(m \cdot s)}$
The density of air at 20ºC (Çengel & Ghajar, 2011)	ρ	$1.204\ \mathrm{kg/m^3}$
The coefficient of air resistance (Naguraka, 2003	C_D	0.4
The angular velocity of the Earth's rotational motion (Alonso & Finn, 1967)	ω	$7.292 \times 10^{-5}\ \mathrm{rad/s}$
The radius of the Earth (Alonso & Finn, 1967)	R_{E}	6.35×10^{6} m

The values used in the calculations are provided in Table 1. It should be noted that since the initial velocity and angle are not important in this study, there are no limitations for analyzing projectile motion for other velocities and angles. If a ball is launched with an initial velocity of $7.0\ \mathrm{m/s}$ at an angle of $45°$ with respect to the horizontal towards the south, the percentage contribution of the external forces above the projectile's acceleration compared to gravitational acceleration is presented in Table 2. According to the results in the mentioned table, the significant factors affecting the projectile's motion are air resistance with a percentage of $\%55.88$ and buoyancy force with a percentage of $\%1.49$, compared to the gravitational force of the Earth. These factors should be taken into account in the projectile's motion. It is worth noting that the effect of the laminar air flow is not only very small compared to gravitational force but also cannot be considered in the studied projectile motion due to having the Reynolds number of 1.87×10^4. The Reynolds number is obtained from $\mathrm{Re} = \rho v L/\mu$ considering the values of Table 1.

In the same way, the greatest effect on the location and time of the projectile's impact with the ground are related to the resistance force of air turbulence and its buoyancy force, respectively.

3. RESULTS AND DISCUSSION

Based on the numerical simulation results using MATLAB, the trajectory of the projectile motion under the influence of external forces in Kabul city is shown in Figures 10 to 13. At first glance, the deviation of the projectile from its intended path due to the effects of centrifugal and Coriolis forces is noticeable. However, upon closer examination, these deviations are found to be very negligible. By examining the time and location of the projectile's collision under the influence of these two forces in Table 2, the matter is well proven.

The effect of air resistance on the trajectory of motion, as well as the time and location of the projectile's collision with the ground and its peak point, is shown in comparison to the effect of gravity alone in Figure 10. It is clearly observed that the motion trajectory lies on a plane.

Table 2**.** Shows the impact of the acceleration factors on the projectile's motion, location, and time of impact with the ground.

Force	Gravitational force of the Earth, $\boldsymbol{F_g}$	Drag force for laminar flow, $\boldsymbol{F_{drag}}$	Drag force for turbulent flow, $\boldsymbol{F_{drag}}$	Buoyancy force, $\boldsymbol{F_b}$	Centrifugal force, $\boldsymbol{F_r}$	Coriolis force, $\boldsymbol{F_c}$
Force equation	$m\mathbf{g}_0$	$-b\boldsymbol{v}$	$-Dv\boldsymbol{v}$	$\rho V \mathrm{g}_0\hat{\mathbf{k}}$	$-\boldsymbol{\omega}\times(\boldsymbol{\omega}\times\boldsymbol{r})$	$-2\boldsymbol{\omega}\times\boldsymbol{V'}$
Projectile acceleration	$\mathbf{g}_0$	$-b\boldsymbol{v}/m$	$-D\boldsymbol{v}^2/m$	$\rho V \mathrm{g}_0/m\hat{\mathbf{k}}$	$-\boldsymbol{\omega}\times(\boldsymbol{\omega}\times\boldsymbol{r})/m$	$-2\boldsymbol{\omega}\times\boldsymbol{V'}/m$
Percentage	%100	%0.18	%55.88	%1.49	%0.28	%0.0086
Impact position(m)	[4.999 0 0]	[4.992 0 0]	[3.553 0 0]	[5.078 0 0]	[5.014 0.008 0]	[4.999 − 0.008 0]
Impact time(s)	1.011	1.011	0.915	1.027	1.014	1.011

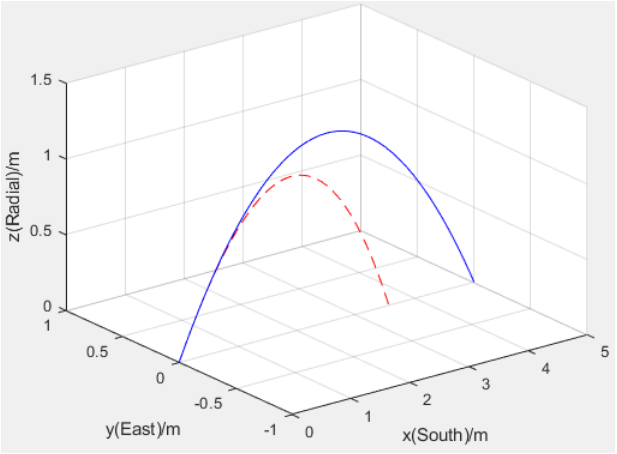

Figure 10. Shows the trajectories of the projectile motion under the influence of only the gravitational force (-) and the force of air resistance (- -) are as follows.

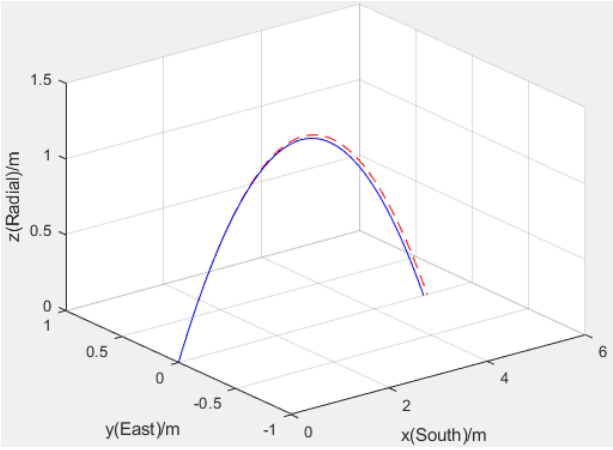

Figure 11**.** Shows the trajectories of the projectile influenced only by the gravitational force (-) and the combined forces of gravity and buoyancy (- -).

As expected, the trajectory of the projectile motion under the influence of buoyancy force in Figure 11 is slightly tilted upwards, but the motion trajectory still lies on a plane.

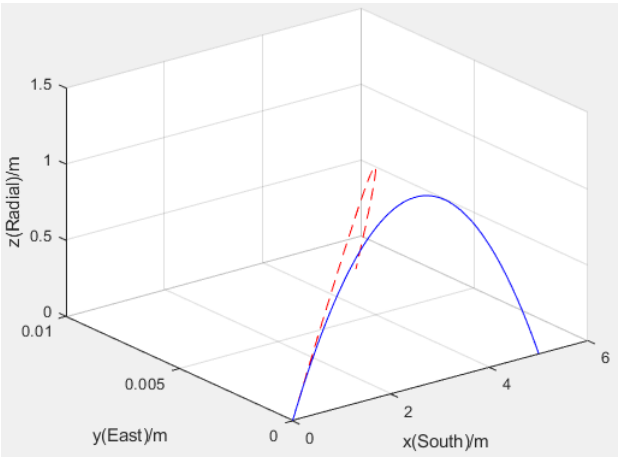

Figure 12. Shows the trajectories of the projectile affected only by the gravitational force (-) and the combined forces of gravity and centrifugal.

As previously mentioned, under the influence of the centrifugal force in the Northern Hemisphere of the Earth, the projectile’s trajectory should be deflected towards the east. This deflection is clearly observed in Kabul city in Figure 12. In other words, the projectile’s motion trajectory under the influence of this force is not confined to a single plane if its effect is significant. However, it should not be mistaken that the deviation of the projectile has occurred due to the effect of this force, which means an 8 mm deviation at the point of impact.

As mentioned earlier, under the influence of the Coriolis force in the Northern Hemisphere of the Earth, the trajectory of the object's motion should be deflected to the right or south. This deflection is clearly observed in Kabul city in Figure 13. In this situation as well, the projectile's motion trajectory does not lie on a single plane if the effect is significant. However, in our case, this effect is very small and can be neglected, resulting in a deviation of only 0.2 mm at the point of collision.

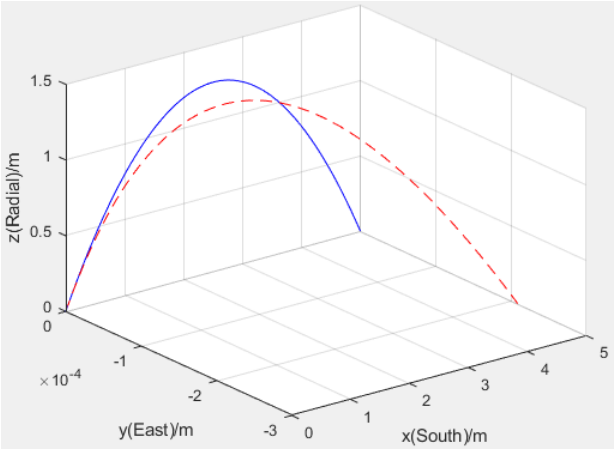

Figure 13**.** Shows the paths of projection motion under just gravitation force (-) and gravitation force and Coriolis force (--).

In the end, the path of the projectile under the influence of the effective forces of gravity, air drag, and buoyancy, compared to the force of gravity alone, is shown in Figure 14b. According to this figure, these forces not only affect the range of the projectile but also result in a significant decrease in its apex point in terms of both location and time. The time and location of the projectile's impact on the ground under the influence of only the force of gravity are $t = 1.011$ s and $\boldsymbol{r} = [4.999\ 0\ 0]^{\mathrm{T}}$ m, respectively, while under the simultaneous effect of the three effective forces, they are $t = 0.928$ s and $\boldsymbol{r} = [3.593\ 0\ 0]^{\mathrm{T}}$ m.

The effect of these two forces, in addition to the force of gravity, accounts for %57.37 of the total impact during the projectile's descent, indicating the significance of considering the influence of these forces on the projectile's motion. In other words, neglecting the effects of these forces would result in a considerable error in estimating the time and location of the projectile's impact. In some research articles (Naguraka, 2003; Tian et al., 2011), the motion of the projectile has been analyzed with the consideration of these effects, leading to acceptable results that can serve as experimental validation for the accuracy of the simulation results obtained in this study.

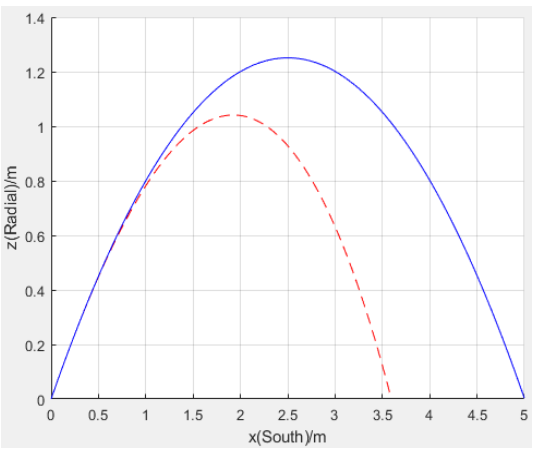


```
tmax = 10; % s
dt = 1e-3; % s
N = tmax/dt;

vc = v0; % m/s
D = 1/2*rho*A*CD;
V = 4/3*pi*R^3;
ml = m - rho*V;
ab = [0 0 -ml/m*g]';

thetaw = -20/180*pi; % Rad
phiw = 40/180*pi; % Rad

n = 1;
r(:, n) = [0 0 0]';
v(:, n) = v0*[cos(theta)*cos(phi)...
    cos(theta)*sin(phi)...
    sin(theta)]'; % m/s
while n < N && r(3, n) >= 0
    a(:, n) = ab - D/m*(v(:, n)'*v(:, n))^0.5*v(:, n);
    v(:, n + 1) = v(:, n) + a(:, n)*dt;
    r(:, n + 1) = r(:, n) + v(:, n)*dt + 1/2*a(:, n)*dt^2;
    n = n + 1;
end
rl(:, 1) = r(1, 1:end-1);
rl(:, 2) = r(3, 1:end-1);
figure
plot(r(1, 1:end-1), r(3, 1:end-1), "--r");
hold on
xlabel("x(South)/m"); ylabel("z(Radial)/m");
grid
```

a) b)

Figure 14. a) Illustrates the paths of the projectile's motion under the influence of gravity alone (-) and under the combined effects of gravity and air drag and buoyancy (- -). b) Sample MATLAB code to get the trajectory of the projectile.

Furthermore, Figure 14a clearly demonstrates that the path of the projectile's motion lies within a plane. While the numerical solution of the non-linear kinematic equations of projectile motion has been straightforward, the analytical solution is highly restrictive, complex, and challenging (Parker, 1997).

In Figure 15, it is clearly seen that the actual path of the projectile's motion, under the influence of gravity, air drag, and buoyancy forces, is well fitted by a second-degree polynomial curve: $z = -0.323\,x^2 + 1.193\,x - 0.062$, which represents a good approximation of a parabola. The obtained impact location from the fitted curve is $\boldsymbol{r} = [3.645\ 0\ 0]^{\mathrm{T}}$ m. The percentage of error in the final position at the point of impact is %1.45.

If the projectile is subjected to a constant wind velocity of $v_{\mathrm{W}} = 2.0$ m/s, making an angle of -20° with the horizontal and towards the east, or if $\boldsymbol{v}_{\mathrm{W}} = [1.44\ 1.208\ -0.604]^{\mathrm{T}}$ m/s in Cartesian coordinates, the plane of the projectile's trajectory will be displaced from its initial position, as shown in Figure 16. However, under the influence of a variable velocity airflow, the trajectory will deviate from the plane and become three-dimensional. If the projectile's motion is within a confined environment, it is possible to reasonably neglect this effect with good accuracy.

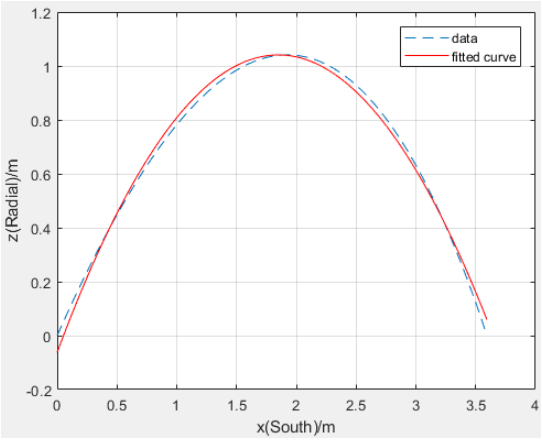

Figure 15. Shows the fitting or alignment of a parabola with the paths of the projectile's motion under the influence of gravity, air drag, and buoyancy forces.

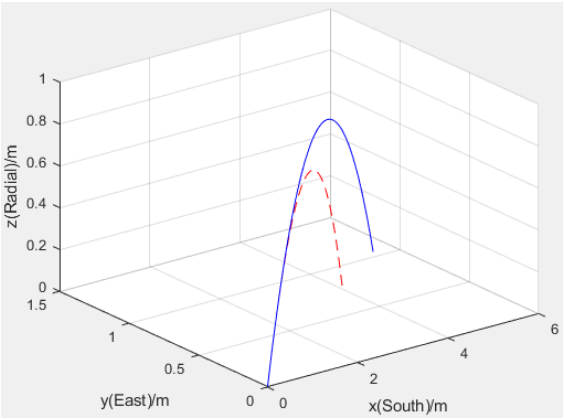

Figure 16. Shows the effect of a constant wind velocity on the paths of the projectile's motion under the influence of gravity only (-) and under the combined effects of gravity,

air drag, and buoyancy forces (- -). The constant wind velocity is not depicted in this figure.

Figure 17 illustrates that considering all factors, including a constant airflow, does not result in a significant change in the projectile's impact location and time in its trajectory. The impact time and location on the ground, under the influence of all three effective forces, are $t = 0.799$ s and $\boldsymbol{r} = [3.959\ 0.747\ 0]^{\mathrm{T}}$ m, respectively. Similarly, under the simultaneous effect of all forces, the impact time and location are $t = 0.801$ s and $\boldsymbol{r} = [3.967\ 0.754\ 0]^{\mathrm{T}}$ m, respectively. This suggests that the inclusion of all these forces does not lead to a noticeable change in the time and location of the projectile's impact.

To validate the accuracy of the numerical method, the analytical and numerical solutions for the velocity and position of the projectile have been compared in specific scenarios. Figure 18 displays a three-dimensional graph of the velocity of a projectile launched with an initial velocity of $7.0\ \mathrm{m/s}$ at an angle of 45° with respect to the horizontal axis (x-axis), under the influence of air resistance.

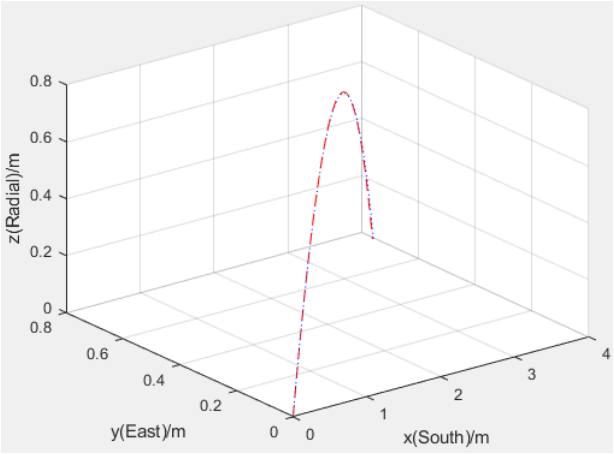

Figure 17. Shows the effect of a constant airflow on the paths of the projectile's motion under the influence of three effective forces (...) and all effective forces combined (- -).

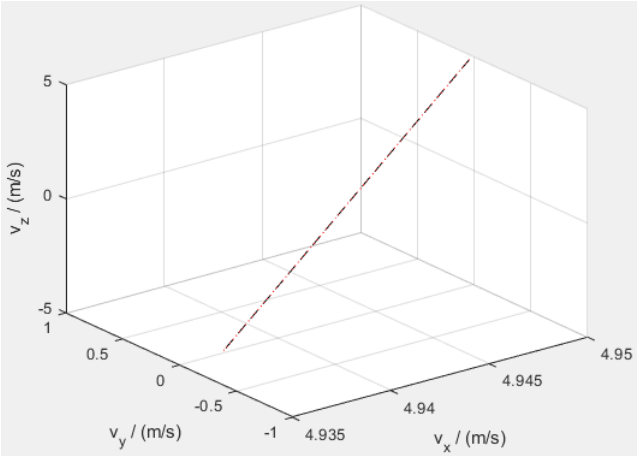

Figure 18. Compares the three-dimensional trajectory of the projectile's velocity under the influence of air resistance using the analytical method (…) and the numerical method (- -).

The velocity of the projectile is considered from the moment of launch until the moment of impact or collision with the ground. The percentage error of the final velocity is $\%1.26 \times 10^{-4}$.The analytical solution for the velocity of the projectile under the effect of air resistance is provided by equation (5). The numerical solution of the motion equations has been performed using a code implemented in MATLAB programming language(Figure 14b), following the algorithm depicted in Figure 19.

In Figure 19, the velocity of an object under the influence of air turbulence has been obtained and compared using both the analytical and numerical methods. The analytical solutions for the projectile's velocity in specific scenarios have been performed according to equations (10), (11), and (12).

Now let's consider the horizontal motion of the object under the influence of air turbulence, starting with an initial horizontal velocity of $7.0\ m/s$. In Figure 20, the graph of its position with respect to time has been obtained and compared using both the analytical and numerical methods. The analytical solution for the projectile's position has been computed according to equation (13). The percentage error of the final position within the given time interval in the figure is $\%0.023$.

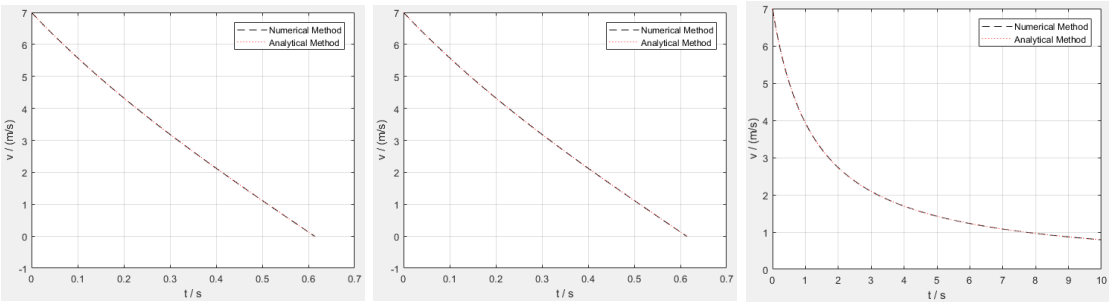

a) b) c)

Figure 19. Comparing the speed of an object under the following conditions: a) Free fall from a height of 3 m, b) Vertical projectile motion, and c) Horizontal motion without considering gravity, under the influence of air resistance, using analytical and numerical methods.

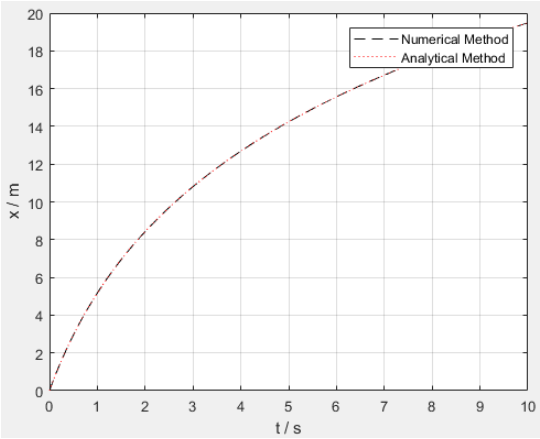

Figure 20. Compares the position of the object in horizontal motion without considering gravity, under the influence of air turbulence, using both the analytical and numerical methods.

4. CONCLUSIONS

Solving linear and nonlinear dynamic equations of inclined projectile motion using numerical methods is both feasible and straightforward. Although solving the motion equations using numerical methods leads to approximate solutions, these results have an acceptable level of accuracy for engineering purposes. In robotics problems, considering the effects of air turbulence and buoyancy force in the dynamic equations of projectile motion is highly important and significant. Estimating the trajectory of projectiles such as a ping-pong ball and determining the location and time of impact with the ground require taking these effects into account. The trajectory of projectile motion is always confined to a plane, and its curve approximates a parabola very well. As a limitation, the results of this study are acceptable for investigating the movement of objects near the Earth's surface where their motion is not influenced by the Earth's rotational motion. However, in conditions where non-inertial forces are present, the trajectory deviates from the plane and becomes three-dimensional. If the airflow has a constant velocity, the plane of the trajectory shifts depending on the direction and magnitude of the velocity. However, if the airflow velocity is variable, the trajectory of the projectile deviates from a plane. Although the analysis of this study has been conducted for a specific velocity and angle, there are no limitations for analyzing projectile motion for other velocities and angles. As a future work, it is hoped that the results of this study can be used to effectively solve the problem of catching projectiles by a robot.

Nomenclature

$\boldsymbol{a}$ = acceleration vector, $\mathrm{m/s^2}$
b = drag coefficient, $\mathrm{kg/s}$
A = the cross-sectional area of the sphere, $\mathrm{m^2}$
C_D = drag coefficient
$\boldsymbol{F}$ = force vector, N
$\mathrm{g_0}$ = acceleration of gravity as measured by a nonrotating observer, $\mathrm{m/s^2}$
g = acceleration of gravity as measured by a rotating observer, $\mathrm{m/s^2}$
L = diameter of the ping pong ball, mm
m = mass of the ping pong ball, g
$\boldsymbol{r}$ = positon vector, m
R = radius of the spherical body, m
Re = the Reynolds number
R_{E} = radius of the Earth, m
t = time, s
$\boldsymbol{v}$ = velocity vector, $\mathrm{m/s}$
V = the spherical body volume, $\mathrm{m^3}$
$\boldsymbol{V'}$ = free fall velocity, $\mathrm{m/s}$
λ = geographic latitude, Degree
μ = dynamic viscosity of air, $\mathrm{kg/(m \cdot s)}$
ρ = density of air, $\mathrm{kg/m^3}$
ω = angular velocity, $\mathrm{rad/s}$

REFERENCES

Alonso, M., & Finn, E. J. (1967). Fundamental university physics (Vol. 2, pp. p-818). Reading, MA: Addison-Wesley.

Anderson, J. D. (2017). Fundamentals of aerodynamics (6th ed.). McGraw-Hill Education.

Batchelor, G. K. (2000). An introduction to fluid dynamics. Cambridge university press.

Bäuml, B., Wimböck, T., & Hirzinger, G. (2010, October). Kinematically optimal catching a flying ball with a hand-arm-system. In 2010 IEEE/RSJ International Conference on Intelligent Robots and Systems (pp. 2592-2599). IEEE.

Bohg, J., Morales, A., Asfour, T., & Kragic, D. (2014). Data-driven grasp synthesis—A survey. IEEE Transactions on Robotics, 30(2), 289–309.

Brancazio, P. J. (1985). Sport science: Physical laws and optimum performance. Simon & Schuster.

Cigliano, P., Lippiello, V., Ruggiero, F., & Siciliano, B. (2015). Robotic ball catching with an eye-in-hand single-camera system. IEEE Transactions on Control Systems Technology, 23(5), 1657-1671.

Çengel, Y. A., & Ghajar, A. J. (2011). Heat and Mass Transfer: Fundamentals and applications, 4th The McGraw-Hill Companies. Inc., New York, NY.

Dickhoff W. H. Projectile Motion with Air Resistance. Retrieved 11 14, 2023, from https://web.physics.wustl.edu/~wimd/topic01.pdf

Elger, D. F., LeBret, B. A., Crowe, C. T., & Roberson, J. A. (2020). Engineering fluid mechanics. John Wiley & Sons.

Frese, U., Bauml, B., Haidacher, S., Schreiber, G., Schäfer, I., Hahnle, M., & Hirzinger, G. (2001, October). Off-the-shelf vision for a robotic ball catcher. In Proceedings 2001 IEEE/RSJ International Conference on Intelligent Robots and Systems. Expanding the Societal Role of Robotics in the the Next Millennium (Cat. No. 01CH37180) (Vol. 3, pp. 1623-1629). IEEE.

Goldstein, H., Poole, C., & Safko, J. (2001). Classical mechanics (3rd ed.). Addison-Wesley.

Greenwood, D. T. (2003). Advanced dynamics. Cambridge University Press.

Halliday, D., Resnick, R., & Walker, J. (2013). Fundamentals of physics. John Wiley & Sons.

Hong, W., & Slotine, J. J. E. (2005, June). Experiments in hand-eye coordination using active vision. In Experimental Robotics IV: The 4th International Symposium,

Stanford, California, June 30–July 2, 1995 (pp. 130-139). Berlin, Heidelberg: Springer Berlin Heidelberg.

Kao, S. T., & Ho, M. T. (2021). Ball-catching system using image processing and an omni-directional wheeled mobile robot. Sensors, 21(9), 3208.

Kao, S. T., Wang, Y., & Ho, M. T. (2017, June). Ball catching with omni-directional wheeled mobile robot and active stereo vision. In 2017 IEEE 26th International Symposium on Industrial Electronics (ISIE) (pp. 1073-1080). IEEE.

Kim, S., Shukla, A., & Billard, A. (2014).Catching objects in flight. IEEE Transactions on Robotics, 30(5), 1049-1065.

Koval, M. C., King, J. E., Pollard, N. S., & Srinivasa, S. S. (2015, September). Robust trajectory selection for rearrangement planning as a multi-armed bandit problem. In 2015 IEEE/RSJ International Conference on Intelligent Robots and Systems (IROS) (pp. 2678-2685). IEEE.

Lai, H. Y., & Ke, H. Y. (2019). Projectile flight trajectory and position estimation system based on stereo vision. Sensors and Materials, 31(11), 3483-3493.

Lippiello, V., Ruggiero, F., & Siciliano, B. (2013). 3D monocular robotic ball catching. Robotics and Autonomous Systems, 61(12), 1615-1625.

Nagurka, M. L. (2003). Aerodynamic effects in a dropped ping-pong ball experiment. International Journal of Engineering Education.

Nathan, A. M. (2008). The effect of spin on the flight of a baseball. American Journal of Physics, 76(2), 119–124.

Nobahar, B., Shoaran, M., & Khosroshahi, G. K. (2020). Ball trajectory estimation and robot control to reach the ball using single camera. Journal of Control, 14(3), 75-87.

Oka, T., Komura, N., & Namiki, A. (2017, October). Ball juggling robot system controlled by high-speed vision. In 2017 IEEE International Conference on Cyborg and Bionic Systems (CBS) (pp. 91-96). IEEE.

Park, G. R., Kim, K., Kim, C., Jeong, M. H., You, B. J., & Ra, S. (2009, September). Human-like catching motion of humanoid using evolutionary algorithm (ea)-based imitation learning. In RO-MAN 2009-The 18th IEEE International Symposium on Robot and Human Interactive Communication (pp. 809-815). IEEE.

Parker, G. W. (1977). Projectile motion with air resistance quadratic in the speed. American Journal of Physics, 45(7), 606-610.

Press, W. H. (2007). Numerical recipes 3rd edition: The art of scientific computing. Cambridge university press.

Redmon, J., Divvala, S., Girshick, R., & Farhadi, A. (2016). You only look once: Unified, real-time object detection. Proceedings of the IEEE Conference on Computer Vision and Pattern Recognition (CVPR), 779–788.

Riley, M., & Atkeson, C. G. (2002). Robot catching: Towards engaging human-humanoid interaction. Autonomous Robots, 12, 119-128.

Tian, J. D., Sun, J., & Tang, Y. D. (2011). Short-baseline binocular vision system for a humanoid ping-pong robot. Journal of Intelligent & Robotic Systems, 64, 543-560.

Xie, Q., Liu, Y., Xiong, R., & Chu, J. (2014, May). Real-time accurate ball trajectory estimation with “asynchronous” stereo camera system for humanoid Ping-Pong robot. In 2014 IEEE International Conference on Robotics and Automation (ICRA) (pp. 6212-6217). IEEE.

Zhang, Z., Cui, Z., Xu, C., Yan, Y., Sebe, N., & Yang, J. (2020). Pattern-affinitive propagation across depth, surface normal and semantic segmentation. IEEE Transactions on Pattern Analysis and Machine Intelligence, 43(10), 3601–3614.